MULTI-SCALE $k-\varepsilon$ MODELLING OF TURBULENCE FOR POROUS MEDIUM FLOWS

Yusuke Kuwata[1] **and Kazuhiko Suga**[2]
Department of Mechanical Engineering,
Osaka Prefecture University,
1-1, Gakuen-cho, Naka-ku, Sakai, Osaka 599-8531, Japan
1: kuwata@htlab.me.osakafu-u.ac.jp
2: suga@me.osakafu-u.ac.jp

ABSTRACT

To predict turbulence in porous media, a new approach is discussed. By double (both volume and Reynolds) averaging Navier-Stokes equations, there appear two unknown covariant terms in the momentum equation. They are namely the dispersive covariance and the volume averaged Reynolds stress which is split into the macro-scale Reynolds stress and the micro-scale Reynolds stress. To obtain the Reynolds stresses, two-equation eddy viscosity models are applied to the volume averaged Reynolds stress and the micro-scale Reynolds stress whilst the Smagorinsky model is applied to the dispersive covariance. The presently proposed multi-scale four-equation $k-\varepsilon$ model is evaluated in porous wall channel flows and porous rib channel flows with good accuracy.

INTRODUCTION

Flows over permeable porous surfaces are commonly encountered in environmental and engineering fluid mechanics. They play important roles in mass and energy exchanges across the interfaces. Treating flows inside and around a highly porous material is thus of primary interest in designing flow passages of fuel cells, catalytic converters and heat sinks, etc. Many research studies were hence historically performed to model and simulate flows inside and near highly permeable walls. Particularly in turbulent flow regimes, since the statistical treatment of the momentum equation produces many unknown multi-scale correlations, relatively crude approaches have been applied to close the equation system. Nakayama & Kuwahara (2008) and Pedras & de Lemos (2001) developed turbulence models based on the $k-\varepsilon$ two equation eddy viscosity model significantly dropping and ignoring many unknown correlations which are insignificant in "homogeneous" regions in porous media.

However, when one considers the interface regions between the porous wall and the outer fluid regions, such ignored terms become non-negligible. Consequently, more precise modelling for turbulence in interface regions is needed for treating flows inside and/or around porous media (Kuwata & Suga, 2013). To develop a turbulence model which is relatively simple, but keeps important multi-scale flow physics, for the flows inside and around porous media, this study develops *four-equation* $k-\varepsilon$ turbulence model.

TURBULENCE MODELLING

Double-averaged Navier-Stokes equations

Following Whitaker (1996), the volume averaging process in the porous media is applied to the Navier-Stokes equations. The volume averaged value $\langle\phi\rangle$ is called the *superficial* averaged value while $\langle\phi\rangle^f$ is the *intrinsic* averaged value of a variable ϕ. Between them, the relation: $\langle\phi\rangle = \varphi\langle\phi\rangle^f$, exists with the porosity of the porous medium φ. When the Reynolds averaging is performed to the volume averaged momentum equation for incompressible flows in porous media, defining the dispersion: $\tilde{\phi} = \phi - \langle\phi\rangle^f$, and the fluctuation of the Reynolds averaging: $\phi' = \phi - \overline{\phi}$, the resultant form can be written as

$$\frac{\partial\langle\overline{u}_i\rangle^f}{\partial t} + \langle\overline{u}_k\rangle^f\frac{\partial\langle\overline{u}_i\rangle^f}{\partial x_k} = -\frac{1}{\rho}\frac{\partial\langle\overline{p}\rangle^f}{\partial x_i} + \frac{\partial}{\partial x_k}\left(\nu\frac{\partial\langle\overline{u}_i\rangle^f}{\partial x_k}\right) - \overline{f}_i$$
$$-\frac{\partial}{\varphi\partial x_k}\varphi(\underbrace{\langle\overline{u_i'u_k'}\rangle^f}_{R^A_{ik}} + \underbrace{\langle\tilde{\overline{u}}_i\tilde{\overline{u}}_k\rangle^f}_{\mathscr{T}_{ik}}) + \underbrace{\frac{\nu}{\varphi}\left(\frac{\partial\varphi}{\partial x_k}\frac{\partial\langle\overline{u}_i\rangle^f}{\partial x_k} + \langle\overline{u}_i\rangle^f\frac{\partial\varphi^2}{\partial x_k^2}\right)}_{g_i^\varphi}, \tag{1}$$

where the drag term f_i consists of the viscous drag and the form drag and is modelled as the Darcy-Forchheimer term. The terms in $\overline{g_i^\varphi}$ arise due to the inhomogeneity of the porous media. The unknown covarient terms: $\langle\tilde{\overline{u}}_i\tilde{\overline{u}}_k\rangle^f$ and $\langle\overline{u_i'u_k'}\rangle^f$, are respectively the dispersive covariance $\mathscr{T}_{ik}$ and the volume averaged Reynolds stress R^A_{ik}. The volume averaged Reynolds stress can be decomposed into the macro-scale stress R_{ij} and the micro-scale stress r_{ij}:

$$R^A_{ij} = \underbrace{\overline{\langle u_i'\rangle^f\langle u_j'\rangle^f}}_{R_{ij}} + \underbrace{\overline{\langle\tilde{u}_i'\tilde{u}_j'\rangle^f}}_{r_{ij}}. \tag{2}$$

In this study, the dispersive covariance $\mathscr{T}_{ij}$ is modelled by the Smagorinsky model as in Kuwata & Suga (2013), whereas the two-equation turbulence modelling which solves the transport equation of turbulence energy and its dissipation rate is applied to the volume averaged stress R^A_{ij} and the micro-scale stress r_{ij}. Thus, the macro-scale stress R_{ij} is calculated by $R_{ij} = R^A_{ij} - r_{ij}$. The eddy viscosity models applied to R^A_{ij} and r_{ij} are

$$R^A_{ij} = \frac{2}{3}k^A\delta_{ij} - \nu_t^A S_{ij}, \qquad \nu_t^A = C_\mu f_\mu\frac{k^{A2}}{\varepsilon^A}, \tag{3}$$

$$r_{ij} = \frac{2}{3}k_m\delta_{ij} - \nu_t^m S_{ij}, \qquad \nu_t^m = C_\mu f_\mu \frac{k_m^2}{\varepsilon_m}, \tag{4}$$

where S_{ij} is the volume averaged strain tensor: $S_{ij} = \frac{\partial\langle\bar{u}_i\rangle^f}{\partial x_j} + \frac{\partial\langle\bar{u}_j\rangle^f}{\partial x_i} - \frac{2}{3}\delta_{ij}\frac{\partial\langle\bar{u}_k\rangle^f}{\partial x_k}$. The total turbulence energy $k^A (= R_{kk}^A/2)$, its dissipation rate ε^A, the micro-scale turbulence energy $k_m (= r_{kk}/2)$ and its dissipation rate ε_m are obtained respectively by solving their transport equations. The coefficient C_μ and the damping function f_μ are as in the Launder-Sharma $k-\varepsilon$ model (1974).

Total k and ε transport equations

The transport equation of k^A is

$$\frac{\partial k^A}{\partial t} + \langle\bar{u}_k\rangle^f\frac{\partial k^A}{\partial x_k} = \mathscr{D}_k + P_k + P_k^d - P_k^t + G_k^\varphi - \varepsilon^A, \tag{5}$$

$$\mathscr{D}_k = \mathscr{D}_k^\nu + \mathscr{D}_k^t + \mathscr{D}_k^p + T_k^{dis}, \tag{6}$$

$$\begin{aligned} T_k^{dis} &= -\frac{\partial}{\partial x_k}\left(\overline{\langle u_i'\rangle^f\langle\tilde{u}_i'\tilde{u}_k'\rangle^f} + \overline{\langle u_i'\rangle^f\langle\tilde{u}_i'\tilde{\bar{u}}_k\rangle^f} + \overline{\langle u_i'\rangle^f\langle\tilde{\bar{u}}_i\tilde{u}_k'\rangle^f}\right), \\ &\quad -\frac{1}{2}\frac{\partial}{\partial x_k}\left(\overline{\langle u_k'\rangle^f\langle\tilde{u}_i'\tilde{u}_i'\rangle^f} + \overline{\langle\tilde{\bar{u}}_k\tilde{u}_i'\tilde{u}_i'\rangle^f}\right), \end{aligned} \tag{7}$$

$$P_k^d = -\left\langle\left(\overline{\tilde{u}_i'\tilde{u}_k'} + \overline{\tilde{u}_i'\langle u_k'\rangle^f}\right)\frac{\partial\tilde{\bar{u}}_i}{\partial x_k}\right\rangle^f, \tag{8}$$

$$P_k^t = -\overline{\langle\tilde{u}_k'\tilde{u}_i\rangle^f\frac{\partial\langle u_i'\rangle^f}{\partial x_k}}, \tag{9}$$

$$\begin{aligned} G_k^\varphi &= \frac{\nu}{\varphi}\left(2\frac{\partial k^A}{\partial x_k}\frac{\partial\varphi}{\partial x_k} + k^A\frac{\partial^2\varphi}{\partial x_k^2}\right) \\ &\quad -\left(\overline{\langle u_i'\rangle^f\langle\tilde{u}_i'\tilde{u}_k'\rangle^f} + \overline{\langle u_i'\rangle^f\langle\tilde{u}_i'\tilde{\bar{u}}_k\rangle^f} + \overline{\langle u_i'\rangle^f\langle\tilde{\bar{u}}_i\tilde{u}_k'\rangle^f}\right)\frac{\partial\varphi}{\varphi\partial x_k} \\ &\quad -\frac{1}{2}\left(\overline{\langle u_i'\rangle^f\langle u_i'\rangle^f\langle u_k'\rangle^f} + \overline{\langle u_k'\rangle^f\langle\tilde{u}_i'\tilde{u}_i'\rangle^f} + \overline{\langle\tilde{\bar{u}}_k\tilde{u}_i'\tilde{u}_i'\rangle^f}\right)\frac{\partial\varphi}{\varphi\partial x_k}. \end{aligned} \tag{10}$$

The terms $\mathscr{D}_k^\nu, \mathscr{D}_k^t, \mathscr{D}_k^p, P_k, \varepsilon^A$ are the molecular diffusion, turbulent diffusion, pressure diffusion, mean shear production and dissipation rate terms of k^A. The terms by the "micro-scale" turbulent dispersion are the turbulent dispersion transport T_k^{dis}, the hetero-porous term G_k^φ, the mean dispersive shear production P_k^d, the turbulent shear production P_k^t, all which need modelling.

The processes including $\mathscr{D}_k^\nu, \mathscr{D}_k^t, \mathscr{D}_k^p$ and the turbulent dispersion transport T_k^{dis} are altogether modelled by the standard gradient diffusion model as

$$\mathscr{D}_k = \frac{\partial}{\partial x_k}\left[\left(\nu + \frac{\nu_t^A}{\sigma_k^A}\right)\frac{\partial k^A}{\partial x_k}\right], \tag{11}$$

where the turbulent Prandtl number is set to $\sigma_k^A = 0.5$. Since $\overline{\langle\tilde{u}_k\tilde{u}_k\rangle^f} = \mathscr{T}_{kk} + r_{kk}$, it is assumed that the dissipation rate of $\overline{\langle\tilde{u}_k\tilde{u}_k\rangle^f}$ is estimated as the sum of the dissipation rates of $\mathscr{T}_{kk}/2$ and r_{kk} with the local equilibrium in the REV. At the limit to the homogeneous flow in the REV, it is assumed that $P_k^d - P_k^t$ balances with the Reynolds averaged micro-scale dissipation rate as in Kuwata & Suga (2013):

$$P_k^d - P_k^t \simeq \varepsilon_m \simeq \left(\overline{P_k^{svs}} - \overline{F_k^{svs}} - \mathscr{E}\right), \tag{12}$$

where $\mathscr{E}$ is the dissipation rate of $\mathscr{T}_{kk}$. The shear production and the drag force production of the sub-volume-scale stresses: $\overline{P_k^{svs}}$ and $\overline{F_k^{svs}}$, are

$$\overline{P_k^{svs}} = \overline{\langle\tilde{u}_i\tilde{u}_k\rangle^f\frac{\partial\langle u_i\rangle^f}{\partial x_k}}, \tag{13}$$

$$\overline{F_k^{svs}} = F_{km} - \overline{f}_k\langle\hat{\bar{u}}_k\rangle^f, \tag{14}$$

where $\langle\hat{\bar{u}}\rangle^f$ indicates the relative velocity to the porous medium. The drag term F_{km} is modelled as

$$F_{km} = \overline{f_k'\langle u_k'\rangle^f} \simeq \left(\frac{\varphi\nu}{K} + \frac{\varphi^2 C_F}{\sqrt{K}}\sqrt{\langle\hat{\bar{u}}_k\rangle^f\langle\hat{\bar{u}}_k\rangle^f}\right)k_M, \tag{15}$$

where K and C_F are respectively the permeability and the Forchheimer coefficient of porous media. In the condition of the homogeneous flow in the REV, the volume averaged velocity gradient vanishes. As the result, the macro-scale turbulence energy k_M is not produced by the macro-scale gradients. Hence, $\overline{P_k^{svs}} = 0$ and $F_{km} = 0$. The resultant form of the subtraction of the turbulent shear production P_k^t from the dispersive mean shear production P_k^d is written as

$$\begin{aligned} P_k^d - P_k^t &\simeq \left(\overline{P_k^{svs}} - \overline{F_k^{svs}} - \mathscr{E}\right) \\ &= C_D'\left(\overline{f}_k\langle\hat{\bar{u}}_k\rangle^f - \mathscr{E}\right). \end{aligned} \tag{16}$$

The model coefficient applied is $C_D' = 1.1 f_2\sqrt{\varphi}$ with $f_2 = \{1-\exp[-(\varphi R_{tm}/100)^{3/2}]\}^{3/2}$ and $R_{tm} = l_m\sqrt{k_m}/\nu$. The micro-scale turbulent length scale l_m is modelled by using the mean pore diameter D_p of a porous medium and the normal distance from the edge of the porous layer y' as

$$l_m = \min\left(0.1\varphi\frac{y'}{D_p}, 0.5D_p\right). \tag{17}$$

The standard gradient diffusion model is applied to the triple moment in G_k^φ. The modelled form of G_k^φ is expressed as

$$G_k^\varphi = \frac{\nu}{\varphi}\left(2\frac{\partial k^A}{\partial x_k}\frac{\partial\varphi}{\partial x_k} + k^A\frac{\partial^2\varphi}{\partial x_k^2}\right) + \frac{\nu_t^A}{\sigma_k^A}\frac{\partial k^A}{\partial x_k}\frac{\partial\varphi}{\varphi\partial x_k}. \tag{18}$$

The modelled transport equation for the isotropic part of the total dissipation rate $\tilde{\varepsilon}^A = \varepsilon^A - 2\nu(\partial\sqrt{k^A}/\partial x_k)^2$ is

$$\begin{aligned} &\frac{\partial\tilde{\varepsilon}^A}{\partial t} + \langle\bar{u}_k\rangle^f\frac{\partial\tilde{\varepsilon}^A}{\partial x_k} = \mathscr{D}_\varepsilon + F_\varepsilon + 2\nu\nu_t^A\left(\frac{\partial\langle\bar{u}_i\rangle^f}{\partial x_j\partial x_k}\right)^2 \\ &+\{C_{\varepsilon1}(P_k + G_k^\varphi) + C_{\varepsilon2}' f_{\varepsilon2}(P_k^d - P_k^t) - C_{\varepsilon2} f_{\varepsilon2}\tilde{\varepsilon}^A\}\frac{\tilde{\varepsilon}^A}{k^A}. \end{aligned} \tag{19}$$

where the standard coefficients $C_{\varepsilon1} = 1.44, C_{\varepsilon2} = 1.92$, $f_{\varepsilon2} = 1 - 0.3\exp(-Rt^2)$ are applied. where the turbulent Reynolds number is $R_t^A = k^{A2}/(\nu\tilde{\varepsilon}^A)$. The coefficient $C_{\varepsilon2}'$ includes the ratio of the total time scale: $\tau_A = k^A/\tilde{\varepsilon}^A$ and the micro time scale based on the mean pore diameter

D_p and k_m: $\tau_p = D_p/\sqrt{k_m}$, that is, $C'_{\varepsilon 2} = 1.92\tau_A/\tau_p$. The term F_ε is modelled by using the the drag term F_{km} as

$$F_\varepsilon = F_{km} C_{\varepsilon 3} \left(\frac{\tilde{\varepsilon}_m}{k_m} - \frac{\tilde{\varepsilon}_M}{k_M} \right), \tag{20}$$

where the model coefficient $C'_{\varepsilon 3} = 3.8[1 - \exp\{-(R_t^A/100)^2\}]$ is used.

Micro-scale k and ε transport equations

The micro-scale turbulence energy k_m is obtained by

$$\frac{\partial k_m}{\partial t} + \langle \overline{u}_k \rangle^f \frac{\partial k_m}{\partial x_k} = \mathscr{D}_{km} + P_{km} + P_k^d + C_{km}^t + F_{km} + G_k^\varphi - \varepsilon_m, \tag{21}$$

$$\mathscr{D}_{km} = \mathscr{D}_{km}^\nu + \mathscr{D}_{km}^t + \mathscr{D}_{km}^p \underbrace{- \frac{1}{2} \frac{\partial}{\partial x_k} \left(\overline{\langle u'_k \rangle^f \langle \tilde{u}'_i \tilde{u}'_i \rangle^f} + \overline{\langle \tilde{\overline{u}}_k \tilde{u}'_i \tilde{u}'_i \rangle^f} \right)}_{T_{km}^{dis}} \tag{22}$$

$$P_{km} = -r_{ik} \frac{\partial \langle \overline{u}_i \rangle^f}{\partial x_k}, \quad P_k^d = -\left\langle \left(\overline{\tilde{u}'_i \tilde{u}'_k} + \overline{\tilde{u}'_i \langle u'_k \rangle^f} \right) \frac{\partial \tilde{\overline{u}}_i}{\partial x_k} \right\rangle^f, \tag{23}$$

$$C_{km}^t = -\overline{\left(\langle \tilde{u}'_i \tilde{u}'_k \rangle^f + \langle \tilde{\overline{u}}_k \tilde{u}'_i \rangle^f \right) \frac{\partial \langle u'_i \rangle^f}{\partial x_k}}, \tag{24}$$

$$G_k^\varphi = \frac{\nu}{\varphi} \left(\frac{\partial (k^A + k_m)}{\partial x_k} \frac{\partial \varphi}{\partial x_k} + \left(2k_m - k^A \right) \frac{\partial^2 \varphi}{\partial x_k^2} \right) - \frac{1}{2} \left(\overline{\langle \tilde{u}'_i \tilde{u}'_i \tilde{u}'_k \rangle^f} + \overline{\langle u'_k \rangle^f \langle \tilde{u}'_i \tilde{u}'_i \rangle^f} + \overline{\langle \tilde{\overline{u}}_k \tilde{u}'_i \tilde{u}'_i \rangle^f} \right) \frac{\partial \varphi}{\varphi \partial x_k}. \tag{25}$$

The diffusion terms $\mathscr{D}_{km}^\nu, \mathscr{D}_{km}^t, \mathscr{D}_{km}^p$ and T_{km}^{dis} are the molecular diffusion, turbulent diffusion, pressure diffusion and turbulent dispersion transport terms, respectively. The production terms P_{km}, P_k^d are the mean shear production term and the mean dispersive shear production term which is also appear in Eq.(9). The energy cascade process is carried out by the macro-micro turbulence cascade term C_{km}^t and the drag term F_{km} .

The diffusion term $\mathscr{D}_{km}$ which includes the turbulent dispersion transport is modelled by the standard gradient diffusion model as

$$\mathscr{D}_{km} = \frac{\partial}{\partial x_k} \left[\left(\nu + \frac{\nu_t^m}{\sigma_k^m} \right) \frac{\partial k_m}{\partial x_k} \right], \tag{26}$$

where the turbulent Prandtl number is $\sigma_k^m = 0.5$. The subtraction of the turbulent shear production from the macro-micro turbulence cascade is written as

$$C_{km}^t - P_k^t = \underbrace{\overline{\langle \tilde{u}_i \tilde{u}_k \rangle^f \frac{\partial \langle u_i \rangle^f}{\partial x_k}}}_{P_k^{svs}} - \langle \overline{\tilde{u}_i \tilde{u}_k} \rangle^f \frac{\partial \langle \overline{u}_i \rangle^f}{\partial x_k}, \tag{27}$$

where $\overline{P_k^{svs}}$ is modelled with the help of Eq.(16) as

$$\overline{P_k^{svs}} \simeq -C_D(\mathscr{E} + \varepsilon_m) + C'_D(F_{km} + \overline{f}_k \langle \hat{\overline{u}}_k \rangle^f). \tag{28}$$

The additional requirement for $C_{km}^t - P_k^t$ is that they should vanish together when the macroscopic turbulent components vanish as indicated by Eq.(10) and (25). Hence, to ensure it a damping function f_1 is applied to the terms as

$$C_{km}^t - P_k^t = \left\{ -C_D(\mathscr{E} + \varepsilon_m) + C'_D(F_{km} + \overline{f}_k \langle \hat{\overline{u}}_k \rangle^f) - (\mathscr{T}_{ik} + r_{ik}) \frac{\langle \overline{u}_i \rangle^f}{\partial x_k} \right\} f_1, \tag{29}$$

where $f_1 = 1 - \exp(-R_t/100)$ with the turbulent Reynolds number $R_t = k_M^2/(\nu \varepsilon_M)$. The coefficients applied are $C_D = 0.2$ and $C'_D = 0.22\sqrt{\varphi}$. The standard gradient diffusion model is applied to the triple moment in G_{km}^φ. The modelled form of G_{km}^φ is expressed as

$$G_{km}^\varphi = \frac{\nu}{\varphi} \left(\frac{\partial (k^A + k_m)}{\partial x_k} \frac{\partial \varphi}{\partial x_k} + \left(2k_m - k^A \right) \frac{\partial^2 \varphi}{\partial x_k^2} \right) + \frac{\nu_t^m}{\sigma_k^m} \frac{\partial k_m}{\partial x_k} \frac{\partial \varphi}{\varphi \partial x_k}. \tag{30}$$

The modelled transport equation for the isotropic part of the micro-scale dissipation rate $\tilde{\varepsilon}_m = \varepsilon_m - 2\nu(\partial\sqrt{k_m}/\partial x_k)^2$ is

$$\frac{\partial \tilde{\varepsilon}_m}{\partial t} + \langle \overline{u}_k \rangle^f \frac{\partial \tilde{\varepsilon}_m}{\partial x_k} = D_{\varepsilon m} + 2\nu\nu_t^m \left(\frac{\partial \langle \overline{u}_i \rangle^f}{\partial x_j \partial x_k} \right)^2 + \left\{ C'_{\varepsilon 1} F_{km} + C_{\varepsilon 1}(P_{km} + G_{km}^\varphi + C_{km}^t) + C''_{\varepsilon 2} f_{\varepsilon 2} P_k^d - C_{\varepsilon 2} f_{\varepsilon 2} \tilde{\varepsilon}_m \right\} \frac{\tilde{\varepsilon}_m}{k_m}. \tag{31}$$

The model coefficients are $C'_{\varepsilon 1} = 1.8\tau_m/\tau_M, C''_{\varepsilon 2} = 1.92\tau_m/\tau_p$ where the micro time-scale τ_m is defined as $\tau_m = k_m/\varepsilon_m$.

Table 1. Parameters of the porous media of Suga *et al.*'s experiments and Breugem *et al.*'s DNS.

case	φ	K/H^2	C_F	D_p/H
#20	0.82	6.20×10^{-6}	0.17	0.030
#13	0.81	9.93×10^{-6}	0.10	0.048
#06	0.80	2.60×10^{-5}	0.095	0.065
E95	0.95	4.75×10^{-5}	0.292	0.0356

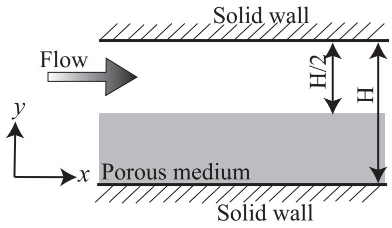

Figure 1. Flow geometry of porous wall channel flows.

RESULTS AND DISCUSSIONS

Porous channel flows

The calibration is performed in flows over porous media (Suga *et al.*, 2010; Breugem *et al.*, 2006). Fig. 1 illustrates the channel flows whose bottom wall is made of a porous medium. The channel height is H and the porous

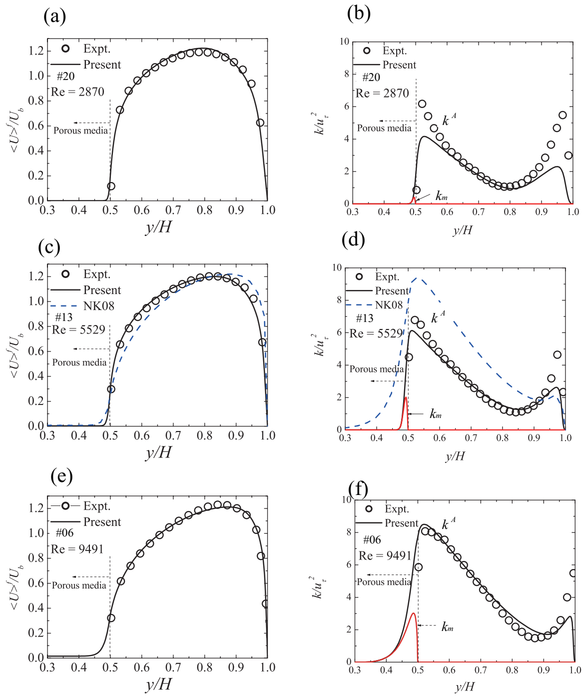

Figure 2. Comparison of velocity and turbulence energy profiles between the prediction and the experiments: (a) velocities in case #20, (b) turbulence energy in case #20, (c) velocities in case #13, (d) turbulence energy in case #13, (e) velocities in case #06, (e) turbulence energy in case #06.

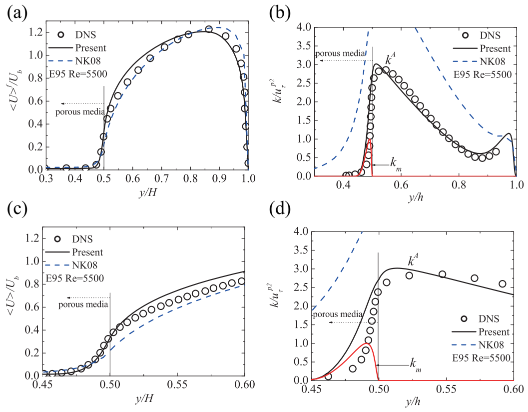

Figure 3. Comparison of velocity and turbulence energy profiles between the prediction and the DNS (case E95): (a) velocities, (b) turbulence energy, (c) near porous wall velocities, (d) near porous wall turbulence energy.

region is up to a half of the channel height $y \leq H/2$. The upper and bottom faces of the channel are solid walls and the periodical boundary conditions are applied to the inlet and outlet boundaries. To evaluate the present model, the results are compared with the experiments of Suga *et al*. (2010) and DNS of Breugem *et al*. (2006). As shown in Table.1, in the experiments, the porosity φ of the porous media is almost constant while their permeability K changes. The most permeable case is case #06 and the least permeable case is case #20 as in Table 1. The bulk Reynolds number is defined as Re$= U_b \frac{H}{2}/\nu$ based on the bulk velocity U_b of the clear channel region.

Fig. 2 compares the mean velocity and turbulence energy profiles of the present model with those of the experiments. The solutions are obtained by an in-house code using the third-order upwind scheme for convection terms. A computational mesh of $30(x) \times 170(y)$ is used. Turbulence energy profiles are normalized by the friction velocity on the top solid wall u_τ. As shown in Fig. 2, the overall agreement in the mean velocities of the present results and the data is satisfactory. In the higher permeable case : case #06, the profiles are very asymmetric and the location of the maximum mean velocity sifts to the solid wall. It is because that the turbulence energy is more produced near the porous wall compared with near the solid wall. This tendency is well captured by the present model. Fig. 3 compares the mean velocity and turbulence energy profiles of the present model with those of the DNS. Turbulence energy are normalized by the friction velocity on the porous wall u_τ^p. As shown in Fig. 3, the prediction of the mean velocity profiles in the porous wall well accords with that of the DNS. Though the peak of the turbulence energy near porous wall is predicted precisely, the turbulence energy is overestimated inside the porous wall.

To confirm the advantage of the present model over an existing model, the results of Nakayama & Kuwahara (2008) (NK08 model) are also plotted in Fig. 2(c),(d) and Fig.3. Although the tendency of the mean velocity and turbulence energy profiles are also reproduced by the NK08 model, the turbulence energy near the porous wall is excessively produced compared with the present results.

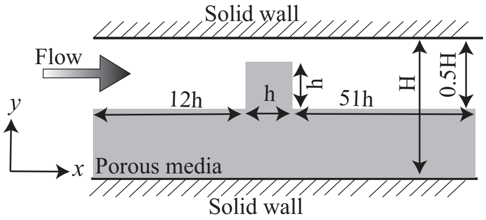

Figure 4. Computational geometry of porous rib channel flows.

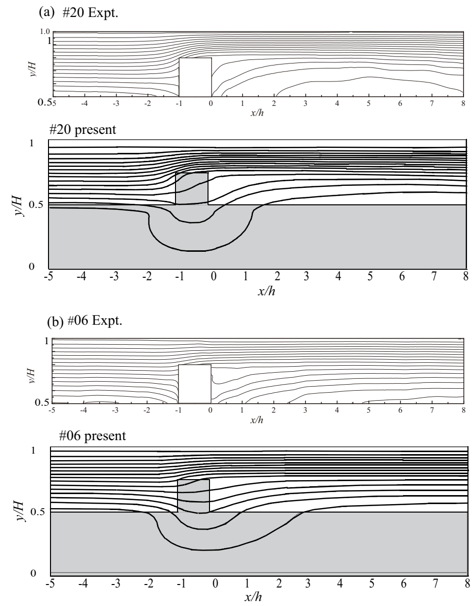

Figure 5. Comparison of the streamlines with the experiments: (a) case #20, (b) case #06.

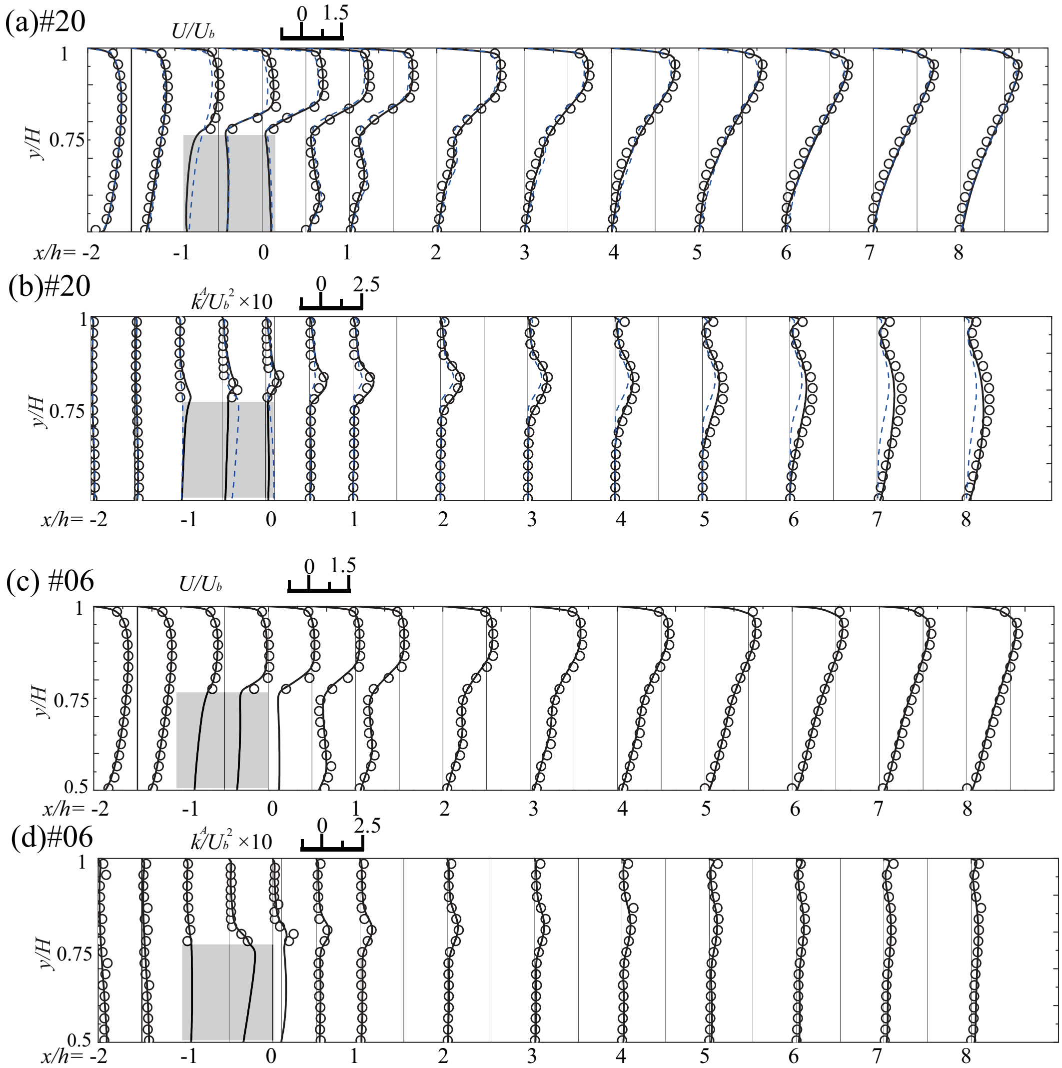

Figure 6. Comparison of the mean velocity and turbulence energy profiles with the experiments: (a) streamwise mean velocity profiles of case #20, (b) turbulence energy profiles of case #20, (c) streamwise mean velocity profiles of case #06, (d) turbulence energy profiles of case #06. Solid lines are the present model; broken lines in (a),(b) are the NK08 model; open circles are from the experiments of Suga *et al.* (2013).

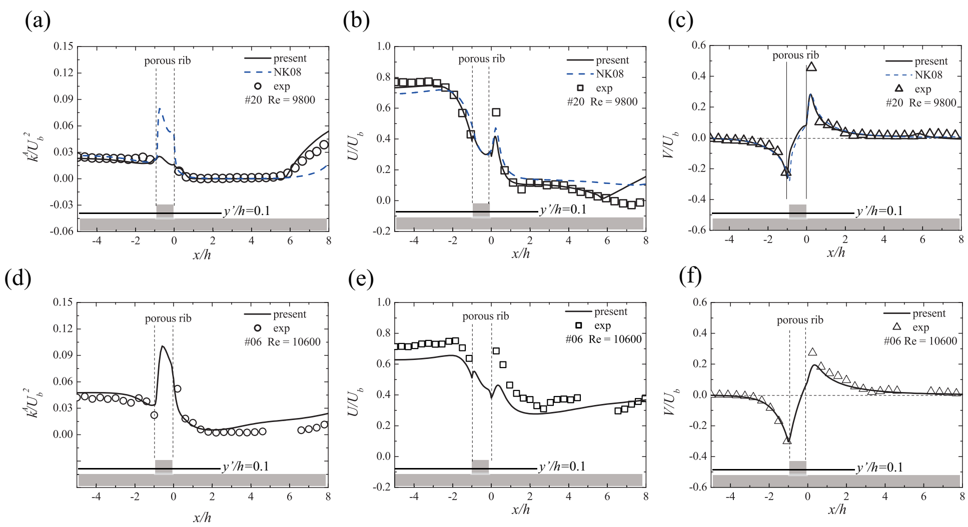

Figure 7. Comparison of the near porous wall profiles: (a) turbulence energy profiles of case #20, (b) streamwise mean velocity profiles of case #20, (c) cross-streamwise mean velocity profiles of case #20, (d) turbulence energy profiles of case #06, (e) streamwise mean velocity profiles of case #06, (f) cross-streamwise mean velocity profiles of case #06.

Porous rib channel flows

The next calibration is performed in the porous rib channel flows shown in Fig. 4. The porous square rib, which is made of the same porous medium as that of the porous wall, is mounted on the porous wall in the channel. The rib height is $h = 0.5H$. The bulk Reynolds numbers are $\mathrm{Re} = U_b \frac{H}{2}/\nu = 9800$ (case #20) and 10600 (case #06). The computational domain extends from $12h$ upstream the rib face and to $51h$ downstream the rib face as shown in Fig. 4. The computational mesh is $237(x) \times 169(y)$ which is confirmed to be fine enough. Fully developed porous channel flow profiles are imposed at the inlet boundary, while the out flow boundary conditions are used at the outlet boundary. The solutions are obtained by the code using the 3rd-order upwind scheme for convection terms. For the evaluation of the present model, the results are compared with the experiments of Suga *et al*. (2013).

Fig. 5 compares the streamlines. Due to the flow going through the porous rib, a recirculating and reattaching zone is not clearly seen in Fig. 5. As the increase of the permeability (case #20 $\rightarrow$ case #06), it is clear that the streamlines behind the rib tend to be flatter and the stagnation flow region tends to disappear. To validate the results quantitatively, Fig. 6 compares the mean velocity and turbulence energy profiles. The profiles of the mean velocity and the turbulence energy generally agree with those of the experiments. It is clear that the flow rate going through the rib increases at $-1 \leq x/h \leq 0$ as the increase of the permeability (Fig. 6 (a) and (c)). This tendency seems to be well captured by the present model, as the agreement in the velocity distributions just behind the rib ($x/h \leq 1$) is reasonable. The turbulence energy of the downstream region becomes smaller in the higher permeability case as shown in Fig. 6 (b) and (d). This tendency is also well predicted by the present model. The difference between the present and the NK08 model results is seen in the region $-1 \leq x/h \leq 0$ of Fig.6(a) and (b). The turbulence energy by the NK08 model tends to be slightly larger than that of the present model and the agreement with the experiments is less satisfactory (Fig.6(b)).

To discuss the prediction performance in detail, the mean velocity and turbulence energy profiles near the porous wall are compared with the experiments in Fig.7. The mean velocity and turbulence energy profiles at $y'/H = 0.1$ are compared. Here, the normal distance from the porous wall is denoted as y'. Whilst the agreement of turbulence energy and the cross-streamwise velocity looks satisfactory for the present results, the present streamwise velocity in the upstream region from the rib of case #06 is a little smaller than the experiments (Fig.7(e)). Also, it is recognized that the present streamwise velocity in the downstream region ($x/h \geq 6$) of case #20 recovers a little faster (Fig.7 (b))). One of the reasons of the former is that the base $k-\varepsilon$ model (Launder-Sharma, 1974) does not work well in the region where such adverse pressure gradients appear. Although the overall agreement of the turbulence energy and the cross-streamwise velocity is also seen for the NK08 model, it doesn't perform well in the downstream region ($x/h > 4$) compared with the present model (Fig.7(a), (b)).

CONCLUSIONS

To predict turbulence around and inside porous media, two kinds of covariances: the dispersive covariance and the volume averaged Reynolds stress which consists of the macro-scale Reynolds stress and the micro-scale Reynolds stress are individually modelled in the present study. To solve the volume averaged Reynolds stress, two-equation eddy viscosity models are applied to the volume averaged (total) Reynolds stress and the micro-scale Reynolds stress whilst the Smagorinsky model is used for the dispersive covariance. In order to close the total turbulence energy and its dissipation rate equations, the additional terms: the turbulent dispersion transport, the turbulent shear production, and the hetero-porous terms are modelled. To close the micro-scale turbulence energy equation, the additional terms in the transport equation: the turbulent dispersion transport, the mean dispersive shear production, the macro-micro turbulence cascade and the hetero-porous terms, are also modelled. The evaluation of the present model confirms that the present method is very promising. The results of the porous channel flows show that the prediction accuracy of the profiles of the mean velocity and the turbulence energy is satisfactory. The overall agreement between the present prediction and the experiments is also satisfactory in the porous rib channel flows, though the present model still inherits some shortcomings from the original two-equation eddy viscosity model.

REFERENCES

Breugem, W. P., Boersma, B. J. and Uittenbogaard, R. E., 2006, “The influence of wall permeability on turbulent channel flow”, *J. Fluid Mech.*, Vol. 562, pp. 35-72.

Getachew, D., Minkowycz, W.J.and Lage, J.L., 2000, “A modified form of the $k-\varepsilon$ model for turbulent flows of an incompressible fluid in porous media”. *Int. J. Heat Mass Transfer*, Vol. 43, pp. 2909-2915.

Kuwata, Y. and Suga, K., 2013, “Modelling turbulence around and inside porous media based on the second moment closure”, *Int. J. Heat Fluid Flow*, Doi 10.1016/j.ijheatfluidflow.2013.03.001.

Launder, B. E. and Sharma, B. I., 1974, “Application of the energy-dissipation model of turbulence to the calculation of flow near a spinning disc”, *Lett. Heat Mass Transfer*, Vol. 1, pp. 131-137.

Nakayama, A. and Kuwahara, F., 1999, “A macroscopic turbulence model for flow in a porous medium”, *J. Fluids Engrg*., Vol. 121, pp. 427-433.

Nakayama, A. and Kuwahara, F., 2008, “A general macroscopic turbulence model for flows in packed beds, channels, pipes, and rod bundles”, *J. Fluids Engrg*., Vol. 130, pp. 101205-1-7.

Pedras, M. H. J. and de Lemos, M. J. S., 2001, “Macroscopic turbulence modeling for incompressible flow through undeformable porous media”, *Int. J. Heat Mass Transfer*, Vol. 44, pp. 1081-1093.

Suga, K., Matsumura, Y., Ashitaka, Y., Tominaga, S. and Kaneda, M., 2010, “Effects of wall permeability on turbulence”, *Int. J. Heat Fluid Flow*, Vol. 31, pp. 974-984.

Suga, K., Tominaga, S., Mori, M. and Kaneda, M., 2013, “Turbulence characteristics in flows over solid and porous ribs mounted on porous walls”, *Flow Turbul. Combust.*, Doi 10.1007/s10494-013-9542-1.

Whitaker, S., 1996, “The Forchheimer equation: A theoretical development”, *Transp. Porous Med*., Vol. 25, pp. 27-61.